

The Enhanced Ferromagnetism of Single-Layer CrX₃ (X=Br and I) by Van der Waals Engineering

Hongxing Li^{1,2}, Yuan-Kai Xu^{1,2}, Kang Lai^{1,2}, and Wei-Bing Zhang^{1,2,*}

1) *School of Physics and Electronic Sciences, Changsha University of Science and Technology, Changsha 410114, People's Republic of China*

2) *Hunan Provincial Key Laboratory of Flexible Electronic Materials Genome Engineering, Changsha University of Science and Technology, Changsha 410114, People's Republic of China*

*Correspondence to: zhangwb@csust.edu.cn

Abstract

The recent experimental discovery of intrinsic ferromagnetism in single-layer CrI₃ opens a new avenue to low-dimensional spintronics. However, the low Curie temperature $T_c \sim 45$ K is still a large obstacle to its realistic device application. In this work, we demonstrate that the T_c and magnetic moment of CrX₃ (X=Br, I) can be enhanced simultaneously by coupling them to buckled two-dimensional Mene (M=Si, Ge) to form magnetic van der Waals (vdW) heterostructures. Our first-principles calculations reveal that n-doping of CrX₃, induced by a significant spin-dependent interlayer charge-transfer from Mene, is responsible for its drastic enhancement of T_c and magnetic moment. Furthermore, the diversified electronic properties including halfmetallicity and semi-conductivity with configuration-dependent energy gap are also predicted in this novel vdW heterostructure, implying their broad potential applications in spintronics. Our study suggests that the vdW engineering may be an efficient way to tune the magnetic properties of 2D magnets, and the Mene/CrX₃ magnetic vdW heterostructures are wonderful candidates in spintronics and nanoelectronics device

Introduction

During the past decades, a large family of 2D materials with outstanding properties have emerged as the excellent candidates in many fields, such as nanoelectronics, catalysis and energy storage.[1-4] Benefit from the atomic flat surface and the absence of dangling bond, it is easy to stack 2D materials vertically to form van der Waals (vdW) heterostructures with novel properties distinct from monolayer components.[5-8] By choosing the components and stacking styles, heterostructures with desired functions can be designed rationally. However, due to the lack of intrinsic magnetism in 2D limit, the application of 2D materials and their vdW heterostructures in spintronics has been hindered.[9-13] To overcome this problem ,extensive experimental and theoretical efforts have been devoted, such as introducing external magnetism into 2D sheet,[9,10] and seeking intrinsic 2D magnetic material.[11-13] Nevertheless, breakthrough was only achieved recently. Single-layer CrI₃ has been identified as a intrinsic Ising ferromagnet with out-of-plane spin direction,[14] which opens a new avenue to the development of low dimensional spintronics devices. CrI₃ is receiving increasing attention for its Ising type ferromagnetism and semi-conductivity, which is also suggested to be used as high-efficient magnetic tunneling barrier. The low dimensional magnetic tunneling junctions composed by few layers CrI₃ and graphene has been fabricated successfully by several groups,[15-18] which demonstrate high tunneling magnetoresistance even up to 1 000 000%. In addition, CrI₃ also provide new opportunity for the

study of new type quasi-particle,[19] and the interaction between magnetism and light.[20] However, the low Curie temperature T_c of 45 K[14] of CrI_3 is still a large obstacle to its realistic device application.

Tuning the property of 2D materials is one of the most important topics in condensed physics and material science. Conventional strategies such as strain and adsorption have been applied widely to manipulate various physical properties of 2D materials including magnetism.[21,22] On the other hand, the proximity effect have also been proved to be an effective way to regulate the properties of 2D materials. The recently rising vdW heterostructures provide an ideal platform to realize the proximity effect. Since the interlayer interaction is predominated by weak vdW interaction, the common and uncontrollable interfacial defect and trap states in conventional heterostructures can be avoided. For example, the spin-orbit coupling of graphene can be enhanced by depositing them on WSe_2 . [23] A recent experiment indicated that a ferromagnetic EuS film in contact with a topological insulator Bi_2Se_3 might show a largely enhanced Curie temperature and perpendicular magnetic anisotropy.[24]

In the present work, we construct a series of magnetic vdW heterostructures composed with the newly discovered 2D magnet CrX_3 ($X=\text{Br}, \text{I}$) and buckled two-dimensional Mene ($M=\text{Si}, \text{Ge}$). Silicene and germanene are wonderful post-IV Dirac materials for their stronger spin-orbit coupling (SOC) than graphene.[25] Although the Mene based vdW heterostructures have also been investigated extensively,[26-34] the magnetic vdW heterostructures that composed by Mene and 2D magnets is still scarce. Our results predicted an enhanced ferromagnetism in CrX_3 by vdW Engineering. In addition, these heterostructures are also found to possess versatile electronic structure.

Calculation method

All spin-polarized density functional calculations are carried out using the Vienna *ab initio* simulation package (VASP)[35,36] within the projected augmented wave (PAW) method[37] and the generalized gradient approximation (GGA) in the Perdew-Burke-Ernzerhof (PBE) implementation.[38] DFT-D2 method proposed by Grimme[39] was adopt to account for the interlayer van der Waals interactions. A vacuum thickness of 15 Å is used to avoid the artificial interaction between images of heterostructures. The cutoff energy of plane wave basis is set to be 500 eV. The atomic position is relaxed until the residual forces on each atom less than 1×10^{-2} eV/Å. Brillouin zone sampling is done by a $9 \times 9 \times 1$ Γ -center mesh.[40]

Results and discussions

The optimized in-plane parameters for CrBr_3 , CrI_3 , silicene and germanene are 6.345, 6.875, 3.845 and 4.017 Å, which are consistent with previous reports.[11,29,41] The Ge/CrI_3 , Si/CrI_3 and Si/CrBr_3 heterostructure slabs are constructed by $\sqrt{3} \times \sqrt{3}$ Mene supercell to match the CrX_3 single-layer, and the lattice mismatch is 1.2%, 3.2% and 5.0%, respectively.

According to the stacking style between Mene and CrX_3 , three high symmetrical positions namely TX, TbX and TuX, are considered in our calculations. Hexagonal rings with different colours are also shown in Figure 1(a) for a clear illustration. For position TX, all M atoms are right above the top of all X atoms. For position TbX/TuX, half M atoms locate above the bottom/upper X atoms. TX can be converted to TbX (TuX) by sliding about 1/3 CrX_3 lattice parameter along zigzag (armchair) direction. Since Mene is bulked, two different configurations

can be constructed at each position. For instance, at TX, we can place the up or down M atom right above upper X atom to form the two configurations labeled as TX_{up} and TX_{dn}. Therefore, there are total six different stacking configurations as shown in Figure 1.

The equilibrium interlayer distance d , and binding energy E_b per M atom of six stacking configurations are listed in Table I and Figure 2. E_b is calculated by $E_b = (E_M + E_{CrX_3} - E_{Heter})/n$, where E_M , E_{CrX_3} , and E_{Heter} are the total energy of Mene, CrX₃ and heterostructure, respectively. As we can see, TbX_{up} is the most energetically favorable configuration for all heterostructures with the largest E_b of 150, 95 and 66 meV for Ge/CrI₃, Si/CrI₃ and Si/CrBr₃, respectively. Ge/CrI₃ and Si/CrBr₃ have strongest and weakest interlayer interaction. However, the interlayer interactions of Mene/CrX₃ are still weaker than the system of Mene/InSe in the same PBE-D2 level.[29] At each position for all heterostructures, the change of E_b and d that result from vertical inversion between up and down M atom is very small, which range from 0.01 Å to 0.11 Å and from 3 meV to 9 meV, respectively.

To gain further insight into the interlayer interaction, we calculate the charge density difference (CDD). As shown in Figure 3, the distinct configurations-dependent charge redistribution of Ge/CrI₃ system can be found, and small structure change can generate different charge redistribution. More interestingly, the vertical inversion between up and down M atoms in heterostructure gives rise to significantly different CDD, although tiny energy change was found above. For example, there is charge accumulation in interlayer space of Ge/CrI₃ with TX_{dn} configuration, but no charge accumulation is found in case of TX_{up}. At TuX_{up}, the Ge atoms and upper I atoms exhibit significant self redistribution, and some charge accumulate at interlayer spaces. However, at TuX_{dn}, there is no charge redistribution at the corresponding spaces. Nevertheless, regardless of the configuration, there is always charge accumulation at Cr atom. We further calculate the charge transfer quantitatively in these heterostructures by Bader charge analysis,[42] which are listed in Table I and Figure 2. We find CrX₃ always get electrons from Mene, and results in n-doping. This is also in accord with the fact that the electron affinity of CrI₃ (CrBr₃), 4.68 eV (4.91 eV), is larger than the work function of germanene (silicene), 4.34 eV (4.64 eV).[43] As the charge redistributions arise in heterostructures, it is interestingly to look into the alteration of the magnetic properties of CrX₃. The average magnetic moments of Cr atoms in heterostructures for different stacking configurations are 3.156, 3.102 and 3.047 μ_B for Ge/CrI₃, Si/CrI₃ and Si/CrBr₃, respectively, larger than the values of 3.098 (3.008) μ_B in single-layer CrI₃ (CrBr₃). The spin-dependent CDD are calculated to uncover the reason, and Figure 3S in SI depict the result for Ge/CrI₃ in TuX_{dn} as a demonstration. We find the Cr atom gain spin-up charge, while the spin-down charge is lost. In single-layer CrX₃, the d electrons of Cr atoms just occupy spin-up direction orbitals.[11] Therefore, the accumulation of spin-up charge results in a larger magnetic moment than pristine CrX₃. This similar situation is also reported in the system of iron(II) phthalocyanine molecule on Bi₂Te₃ substrate, in which the molecular magnetic moment will increase as charge transfer from substrate.[44] On the other hand, Mene was magnetized due to proximity effect, and Ge atoms can acquire a largest magnetic moment of 0.035 μ_B that antiparallel to Cr atom at TuX_{up} in Ge/CrI₃. This value is much larger than the 0.003 μ_B of Se atom in Bi₂Se₃/CrI₃. [45] In order to determine the magnetic ground state and evaluate magnetic stability of CrX₃, we calculate the exchange energy ΔE of CrX₃ in heterostructure, $\Delta E = E_{AFM} - E_{FM}$. The results are listed in Table 1 and Figure 3(d). The ΔE of single-layer CrX₃ was also calculated, and the result is 39(29) meV for CrI₃ (CrBr₃). As we can see, ΔE varies with systems and

configurations, and range from 53 to 61, 38 to 41, 47 to 53 meV for Ge/CrI₃, Si/CrI₃ and Si/CrI₃, respectively. The ΔE of CrX₃ in the heterostructures is usually larger than the freestanding single-layer one. Compared with free-standing single-layer CrX₃, ΔE in Ge/CrI₃ can increase maximally by 56% at TbX_{up} and TuX_{up}, and in Si/CrBr₃ it can increase maximally by 83% at TuX_{dn}. According to mean-field theory, the Curie temperature T_c is expected to be proportional to ΔE . Using the experimental T_c of single-layer CrI₃ 45 K,[14] the highest T_c of CrI₃ is evaluated to 70 K, close to the liquid nitrogen temperature. It is worthy to note that the ΔE of Ge/CrI₃ is always larger than Si/CrI₃, indicating the overlaying of germanene on CrI₃ will lead to a more stable ferromagnetism than silicene. The enhancement of ferromagnetism in heterostructures can be ascribed to charge transfer from Mene to 2D magnets as discussed above. This is consistent with previous study of Wu et al.,[46] in which they found the charge doping can steadily enhance the ferromagnetism of CrI₃. The similar enhancement of ferromagnetism in magnetic single-layer induced by substrate is also found in the case of VSe₂/MoS₂ by experiment recently.⁴⁷

We also calculate the density of states (DOS) of these systems at different configurations. The DOS of Ge/CrI₃ for six configurations are presented in Figure 4 and other configuration can be found in Figure S4 and S5 in SI. Compared with the single-layer CrX₃, the fermi level of these heterostructures moves toward to conduction band, confirming the n-doping. The M p states hybrid with Cr d and X p states, as they show some identical peaks. However, the top of valence band is dominated by Ge p states, while the bottom of conduction band is dominated by Cr d and X p states. The Dirac cone of Mene was destroyed seriously, even similar to the situation on metal substrate.[26-28] Nevertheless, it is very different from Mene on other non-magnetic insulating 2D substrates, such as MoS₂, WSe₂ and MX (M=Ga, In; X=S, Se, Te).[29-32] The Dirac cone of Mene was found to be well preserved, even though the binding strength between Mene and these substrates may be stronger than on CrX₃. Unlike on usual nonmagnetic substrates, the DOS in spin up and down channels of Mene around Fermi level are asymmetrical and exhibiting strong spin polarizations, as a consequence of magnetic proximity effect. Therefore, in addition to hybridization and asymmetrical potential, the exchange splitting induced by ferromagnetic substrate may be another reason for the destroying of Dirac cone. The spin-polarized band structures of these heterostructures are calculated to understand the electronic properties of heterostructures. The band structures are shown in SI, and we summarize the characters of all band structures in Figure 5. As we can see, the band structures of each system at different configurations show significant difference. For example, Ge/CrI₃ manifest as semiconductor with a band gap of 165 meV at TX_{up}, while at TbX_{up} it become a half-metal with a spin gap of 200 meV. At TX_{dn}, Ge/CrI₃ is semiconductor with a rather small band gap of 25 meV, the 1/6 times as TX_{up}. However, the structural difference between TX_{up} and TX_{dn} is just the inversion of up and down Ge atoms. Apart from semiconductor and halfmetal, Ge/CrI₃ can be metal at TuX_{dn}. Si/CrI₃ can be metal and semiconductor, and the largest gap is 218 meV at TX_{up} and the smallest one is 54 meV at TbX_{up}. Different from Ge/CrI₃ and Si/CrI₃, Si/CrBr₃ is always half-metallic, but the spin gap vary with stacking configuration. At TbX_{dn}, Si/CrBr₃ has smallest spin gap of 35 meV, and the largest gap is 290 meV at TuX_{dn}. The strong configurations-dependent electronic properties of heterostructures are also in consistent with the fact that the CDD changes discussed above.

Summary

In summary, the first principle calculations are employed to study the structural, magnetic and electronic properties of Ge/CrI₃, Si/CrI₃ and Si/CrBr₃ magnetic vdW heterostructures. Electrons will transfer from Mene to CrX₃, leading to n-doping in CrX₃. The n-doping will enhance the ferromagnetism of 2D magnets, as exchange energy of CrI₃ and CrBr₃ increased maximally by 56% and 83%, respectively. The T_c of CrI₃ can increase to 70 K. Our study indicates the van der Waals engineering may be an effective way to tune the magnetic and structure property of 2D magnet. Moreover, the electronic structures of these heterostructures show strong dependence on stacking configurations, as they can be metal, or semiconductor and half-metal with different band gaps. The multiple properties make these magnetic vdW heterostructures have diversified potential applications in spintronics and nanoelectronics.

ACKNOWLEDGMENTS

This work was supported by National Natural Science Foundation of China (Grant No.11847147 and No.11874092) the Fok Ying-Tong Education Foundation, China (Grant No. 161005), the Planned Science and Technology Project of Hunan Province (Grant No. 2017RS3034), Hunan Provincial Natural Science Foundation of China (Grant No. 2016JJ2001), and Scientific Research Fund of Hunan Provincial Education Department (Grant No. 16B002).

Reference

- [1] D. Jariwala, V. K. Sangwan, L. J. Lauhon, T. J. Marks, and M. C. Hersam, ACS Nano **8**, 1102 (2014).
- [2] B. Anasori, M. R. Lukatskaya, and Y. Gogotsi, Nat. Rev. Mater. **2** (2017).
- [3] D. Deng, K. S. Novoselov, Q. Fu, N. Zheng, Z. Tian, and X. Bao, Nat. Nanotechnol. **11**, 218 (2016).
- [4] G. Xie, Z. Ju, K. Zhou, X. Wei, Z. Guo, Y. Cai, and G. Zhang, npj Computational Materials **4**, 21 (2018).
- [5] K. S. Novoselov, A. Mishchenko, A. Carvalho, and A. H. Castro Neto, Science **353** (2016).
- [6] W. Yu, Z. Zhu, S. Zhang, X. Cai, X. Wang, C.-Y. Niu, and W.-B. Zhang, Appl. Phys. Lett. **109**, 103104 (2016).
- [7] K. Lai, C.-L. Yan, L.-Q. Gao, and W.-B. Zhang, J Phys. Chem. C **122**, 7656 (2018).
- [8] K. Lai, H. Li, Y.-K. Xu, W.-B. Zhang, and J. Dai, Phys. Chem. Chem. Phys. (2019), 10.1039/C8CP07298A.
- [9] Y. Cheng, Z. Zhu, W. Mi, Z. Guo, and U. Schwingenschlogl, Phys. Rev. B **87**, 100401 (2013).
- [10] Y.-W. Son, M. L. Cohen, and S. G. Louie, Nature **444**, 347 (2006).
- [11] W.-B. Zhang, Q. Qu, P. Zhu, and C.-H. Lam, J. Mater. Chem. C **3**, 12457 (2015).
- [12] X. Li and J. Yang, J. Mater. Chem. C **2**, 7071 (2014).
- [13] M. Ashton, D. Gluhovic, S. B. Sinnott, J. Guo, D. A. Stewart, and R. G. Hennig, Nano Lett. **17**, 5251 (2017).
- [14] B. Huang, G. Clark, E. Navarro-Moratalla, D. R. Klein, R. Cheng, K. L. Seyler, D. Zhong, E. Schmidgall, M. A. McGuire, D. H. Cobden, W. Yao, D. Xiao, P. JarilloHerrero, and X. Xu, Nature **546**, 270 (2017).
- [15] Z. Wang, I. Gutierrez-Lezama, N. Ubrig, M. Kroner, M. Gibertini, T. Taniguchi, K. Watanabe, A. Imamoglu, E. Giannini, and A. F. Morpurgo, Nat. Commun. **9**, 2516 (2018).
- [16] D. R. Klein, D. MacNeill, J. L. Lado, D. Soriano, E. Navarro-Moratalla, K. Watanabe, T. Taniguchi, S. Manni, P. Canfield, J. Fernández-Rossier, and P. Jarillo-Herrero, Science **360**, 1218

- (2018).
- [17] T. Song, X. Cai, M. W.-Y. Tu, X. Zhang, B. Huang, N. P. Wilson, K. L. Seyler, L. Zhu, T. Taniguchi, K. Watanabe, M. A. McGuire, D. H. Cobden, D. Xiao, W. Yao, and X. Xu, *Science* (2018), 10.1126/science.aar4851.
- [18] H. H. Kim, B. Yang, T. Patel, F. Sfigakis, C. Li, S. Tian, H. Lei, and A. W. Tsen, *Nano Letters* **18**, 4885 (2018).
- [19] S. S. Pershoguba, S. Banerjee, J. C. Lashley, J. Park, H. ° Agren, G. Aeppli, and A. V. Balatsky, *Phys. Rev. X* **8**, 011010 (2018).
- [20] K. L. Seyler, D. Zhong, D. R. Klein, S. Gao, X. Zhang, B. Huang, E. Navarro-Moratalla, L. Yang, D. H. Cobden, M. A. McGuire, *et al.*, *Nat. Phys.* **14**, 277 (2018).
- [21] Y. Guo, S. Yuan, B. Wang, L. Shi, and J. Wang, *J. Mater. Chem. C* **6**, 5716 (2018).
- [22] F. Zheng, J. Zhao, Z. Liu, M. Li, M. Zhou, S. Zhang, and P. Zhang, *Nanoscale* **10**, 14298 (2018).
- [23] A. Avsar, J. Y. Tan, T. Taychatanapat, J. Balakrishnan, G. Koon, Y. Yeo, J. Lahiri, A. Carvalho, A. Rodin, E. O'Farrell, *et al.*, *Nature communications* **5**, 4875 (2014).
- [24] F. Katmis, V. Lauter, F. S. Nogueira, B. A. Assaf, M. E. Jamer, P. Wei, B. Satpati, J. W. Freeland, I. Eremin, D. Heiman, *et al.*, *Nature* **533**, 513 (2016).
- [25] A. Molle, J. Goldberger, M. Houssa, Y. Xu, S.-C. Zhang, and D. Akinwande, *Nature materials* **16**, 163 (2017).
- [26] R. Quhe, Y. Yuan, J. Zheng, Y. Wang, Z. Ni, J. Shi, D. Yu, J. Yang, and J. Lu, *Sci. Rep.* **4**, 5476 (2014).
- [27] N. Gao, H. Liu, S. Zhou, Y. Bai, and J. Zhao, *J Phys. Chem. C* **121**, 5123 (2017).
- [28] L. Y. B. H. Fengping Li, Wei Wei and Y. Dai, *J Phys D: Appl Phys* **50**, 115301 (2017).
- [29] Y. Fan, X. Liu, J. Wang, H. Ai, and M. Zhao, *Phys. Chem. Chem. Phys.* **20**, 11369 (2018).
- [30] L. Zhang, P. Bampoulis, A. N. Rudenko, Q. Yao, A. van Houselt, B. Poelsema, M. I. Katsnelson, and H. J. W. Zandvliet, *Phys. Rev. Lett.* **116**, 256804 (2016).
- [31] Z. Ni, E. Minamitani, Y. Ando, and S. Watanabe, *Phys. Chem. Chem. Phys.* **17**, 19039 (2015).
- [32] J. Zhu and U. Schwingenschlogl, *J Mater. Chem. C* **3**, 3946 (2015).
- [33] M. Chen and M. Weinert, *Phys. Rev. B* **98**, 245421 (2018).
- [34] M. Chen and M. Weinert, *Nano letters* **14**, 5189 (2014).
- [35] G. Kresse and J. Hafner, *Phys. Rev. B* **47**, 558 (1993).
- [36] G. Kresse and J. Furthmüller, *Phys. Rev. B* **54**, 11169 (1996).
- [37] G. Kresse and D. Joubert, *Phys. Rev. B* **59**, 1758 (1999).
- [38] J. P. Perdew, K. Burke, and M. Ernzerhof, *Phys. Rev. Lett.* **77**, 3865 (1996).
- [39] S. Grimme, *J Comput. Chem.* **27**, 1787 (2006).
- [40] H. J. Monkhorst and J. D. Pack, *Phys. Rev. B* **13**, 5188 (1976).
- [41] W.-B. Zhang, Z.-B. Song, and L.-M. Dou, *J. Mater. Chem. C* **3**, 3087 (2015).
- [42] G. Henkelman, A. Arnaldsson, and H. Jónsson, *Computational Materials Science* **36**, 354 (2006).
- [43] M. X. Chen, Z. Zhong, and M. Weinert, *Phys. Rev. B* **94**, 075409 (2016).
- [44] Y. R. Song, Y. Y. Zhang, F. Yang, K. F. Zhang, C. Liu, D. Qian, C. L. Gao, S. B. Zhang, and J.-F. Jia, *Phys. Rev. B* **90**, 180408 (2014).
- [45] Y. S. Hou and R. Q. Wu, (2018), arXiv:1802.07358.
- [46] H. Wang, F. Fan, S. Zhu, and H. Wu, *EPL (Europhysics Letters)* **114**, 47001 (2016).

[47] M. Bonilla, S. Kolekar, Y. Ma, H. C. Diaz, V. Kalappattil, R. Das, T. Eggers, H. R. Gutierrez, M.-H. Phan, and M. Batzill, Nat. Nanotechnol. **13**, 289 (2018).

Table 1 The calculated adsorption energy E_b per M atom, in meV, and interlayer distance d , in Å, and charge transfer $\Delta\rho$, in e, from Mene to CrX_3 , and exchange energy ΔE , in meV, of CrX_3 in heterostructures, for each system at different stacking configurations.

	Ge/CrI_3				Si/CrI_3				Si/CrBr_3			
	E_b	d	$\Delta\rho$	ΔE	E_b	d	$\Delta\rho$	ΔE	E_b	d	$\Delta\rho$	ΔE
Hol_up	111,	3.26,	0.119	56	61,	3.52,	0.078,	38	35,	3.32,	0.116,	48
Hol_dn	102,	3.27,	0.108,	58	64,	3.63,	0.067,	40	38,	3.40,	0.141,	51
TbX_up	150,	3.04,	0.115,	61	95,	3.17,	0.082,	43	55,	3.08,	0.125,	52
TbX_dn	141,	3.05,	0.112,	59	92,	3.20,	0.077,	41	52,	3.11,	0.125,	49
TuX_up	109,	3.36,	0.130,	61	68,	3.55,	0.097,	41	38,	3.24,	0.185,	47
TuX_dn	115,	3.23,	0.142,	53	64,	3.50,	0.091,	36	43,	3.27,	0.123,	53

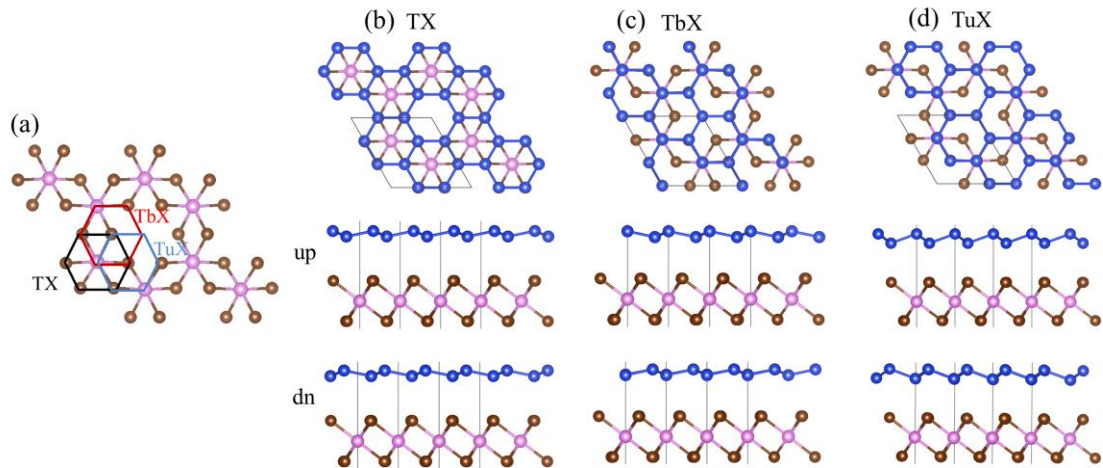


Figure 1 (a) Schematic diagram of three positions for hexagonal ring of Mene located on CrX_3 , (b)(c)(d) the first row, top views of heterostructures at position TX, TbX and TuX; the second and third row, side views of up and down M atom right above top X or Cr atom. The Cr, X, and M atoms are colored by pink, brown and blue.

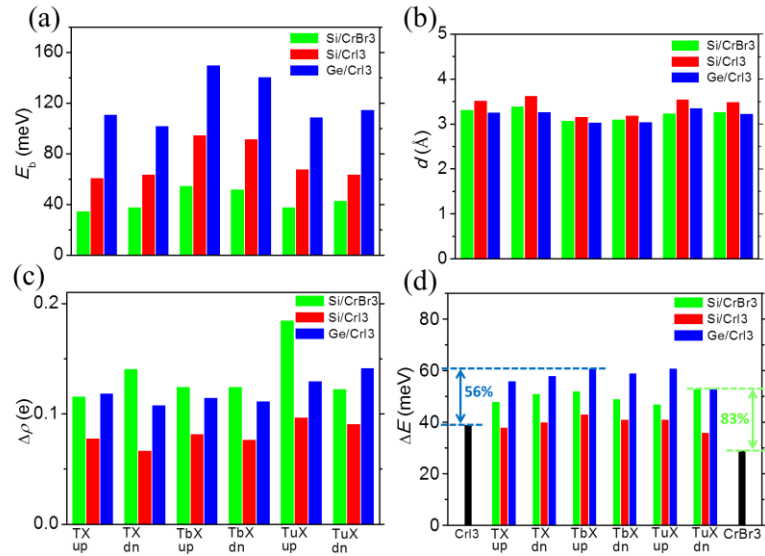


Figure 2 (a) The calculated adsorption energy E_b per M atom, (b) interlayer distance d , (c) charge transfer from Mene to CrX_3 and (d) exchange energy ΔE , for each system at different stacking configurations.

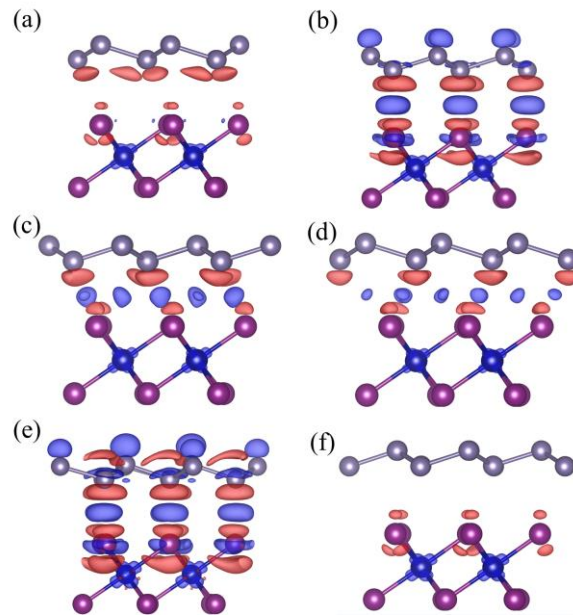


Figure 3 Charge difference density of Ge/CrI_3 for difference configuration (a)(b) $\text{TX}_{\text{up/dn}}$, (c)(d) $\text{TbX}_{\text{up/dn}}$, (e)(f) $\text{TuX}_{\text{up/dn}}$. The blue and red represent the charge accumulation and depletion, the isosurface is set as $0.0005 \text{ eV}/\text{\AA}^3$.

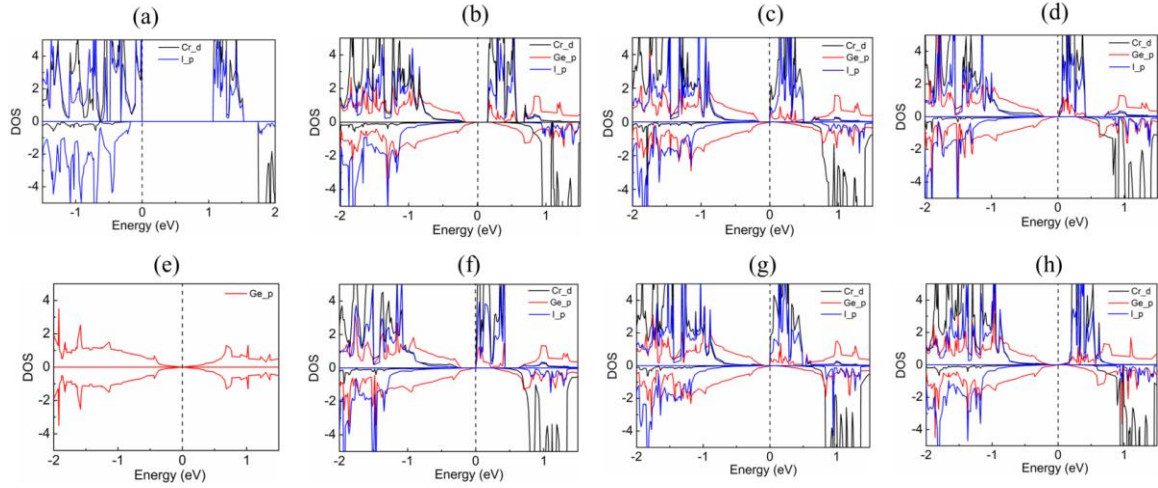


Figure 4 The projected density of states (DOS) for Ge/CrI₃ at different configurations, (b)(f) TX_{up}/dn, (c)(g) TbX_{up}/dn, (d)(h) TuX_{up}/dn. (a)(e) the DOS of single-layer CrI₃ and germanene.

	TX _{up}	TX _{dn}	TbX _{up}	TbX _{dn}	TuX _{up}	TuX _{dn}
Si/CrBr ₃	190	221	110	35	290	170
Si/CrI ₃	218	143	54		76	
Ge/CrI ₃	165	25	200	76	215	

Semiconductor
 Half-metal
 Metal

Figure 5 The characters of band structures for Ge/CrI₃, Si/CrI₃ and Si/CrBr₃ at different configurations. The number is the gap value, blue, green and red represent semiconductor, half-metal and metal, respectively